International Journal of Hydrogen Energy 111 (2025) 723–734

Contents lists available at ScienceDirect

International Journal of Hydrogen Energy

journal homepage: www.elsevier.com/locate/he

Ultrasound-driven seawater splitting catalysed by TiO_2 for hydrogen production

Cherie C.Y. Wong, Davide Bernardo Preso, Yi Qin, Pankaj S. Sinhmar, Zhiyuan Zong, James Kwan *

Department of Engineering Science, Parks Road, Oxford, OX1 3PJ, UK

ARTICLE INFO

Handling Editor: Dr C O Colpan

Keywords:
Hydrogen production
Sonochemistry
Sonocatalysis
Green hydrogen
Seawater splitting

ABSTRACT

Seawater splitting presents a promising approach for sustainable hydrogen production, yet its application remains limited by competing side reactions and expensive catalyst in electrolysis. In this study, we present an alternative hydrogen production approach using ultrasonic-driven seawater splitting catalysed by TiO_2 at room temperature. The application of high-frequency ultrasound (780 kHz, 5.1 W) with a bespoke sonoreactor, designed to focus pulsed ultrasound waves, induces inertial cavitation and generates highly reactive radicals to produce hydrogen. By optimising acoustic parameters and TiO_2 catalyst concentration of 0.3 mg/mL, the system achieved the highest reported sonochemical efficiency for hydrogen production in both pure and natural seawater, reaching 8086 and 4210 μmol g_{cat}^{-1} L^{-1} Whr^{-1}, respectively. We further investigated the significant decrease in hydrogen production in salty environments. Through bubble dynamics simulations and electron paramagnetic resonance measurements, we attributed the salt-scavenging chemical effect has a dominant role in reducing the efficiency. Our findings demonstrate the potential of sonocatalytic seawater splitting with TiO_2 as a viable alternative for renewable hydrogen production.

1. Introduction

Hydrogen is a pivotal energy vector in the transition towards a net-zero world by 2050. As a versatile chemical, it can be used as fuel and feedstock directly in transportation and industrial sectors, or indirectly as an energy vector for electricity generation. Additionally, when hydrogen is combusted, it releases heat for residential or commercial purposes, yielding only water as a by-product. By developing technologies for water splitting using renewable energy to produce hydrogen, the implementation of a circular hydrogen economy becomes feasible [1,2]. As illustrated in Fig. 1, this process involves the sustainable production of hydrogen and its integration into various applications, forming a circular economy that supports green energy transition. Direct seawater electrolysis has attracted significant interest as a technology for hydrogen evolution because of its abundant availability [3,4]. However, several major technological challenges are hindering the full adoption of the technology. First, the electrode surface of conventional electrolysers composed of noble-based materials, including platinum and iridium [5,6], which act as catalyst. These noble metals are scarce and expensive, making the infrastructure of industrial-scale electrolyser economically unsustainable. Moreover, the complex composition of seawater leads to unwanted side reactions on the electrodes: organic compounds contribute to the formation of undesirable biofouling and biofilms, while inorganic metal ions excessively deposit on the electrodes as insoluble precipitates, physically blocking the reaction surface [7–9]. Furthermore, the presence of chlorine ions in seawater triggers toxic chlorine formation and poisoning of the catalyst [10]. These combined effects reduce the overall electrolysis performance and require frequent replacement of catalysts. As an alternative water splitting technique, photocatalytic seawater splitting suffers from poor quantum efficiency and stability of photocatalyst in a salty environment [11]. In this study, we explore sonochemical hydrogen production, or sonohydrogen, as an alternative technique for clean hydrogen production, leveraging ultrasonic inertial cavitation to facilitate seawater splitting.

Sonohydrogen is generated from ultrasound-driven direct hydrolysis, also known as sonolysis. It serves as an alternative approach to generate clean hydrogen as the system operates without CO_2 emission. Sonolysis, the breakdown of water molecule by ultrasound waves, originates from the collapse of acoustic-induced cavitation. Under

* Corresponding author.
E-mail address: james.kwan@balliol.ox.ac.uk (J. Kwan).

https://doi.org/10.1016/j.ijhydene.2025.02.327
Received 10 December 2024; Received in revised form 17 February 2025; Accepted 20 February 2025
Available online 27 February 2025

certain acoustic conditions, cavitation may be purely inertial, allowing for the violent growth and implosion of the gas-vapour bubble [12]. The rapid collapse of these bubbles yields a localised hotspot with extreme temperature and pressure, in the order of magnitude of ~10^3 °C and GPa, respectively [13]. These extreme conditions make each cavity act as a micro-reactor in which the trapped water molecules split to give radical species, e.g., H•, •OH, HO_2•. A fraction of these radicals recombines to form molecular hydrogen. The main reaction pathway of sonochemical hydrogen production is illustrated in Fig. 1 [14]. Hydroxyl radicals may also recombine to form hydrogen peroxide, which accumulates in solution as inertial cavitation proceeds [15]. While hydrogen peroxide formation is an important reaction in some sonochemical systems, it is omitted from Fig. 1 as this study focuses specifically on hydrogen production rather than peroxide chemistry.

Sonolysis offers numerous advantages compared to electrolysis and photocatalysis. First, sonolysis is not a surface-driven reaction as compared to electrolysis, allowing for volumetric scaling. This further prevents instrumental corrosion such as biofouling and deposition [16]. Sonolysis also operates at room temperature, providing a more energy- and cost-effective approach as compared to some thermal-assisted photocatalytic hydrogen production, which typically operates at 100–300 °C [17,18]. Moreover, sonolysis was proven to be more efficient than some conventional technologies. For example, Gentili et al. (2009) and Penconi et al. (2015) have shown that sonolysis of pure water is 100–200 times more efficient than photocatalysis [19,20].

Sonochemical hydrogen production has the potential to serve as a green hydrogen production pathway if integrated with renewable energy sources such as solar or wind power. Despite the potential, this research area is still at its nascent stage with a limited number of works demonstrating the concept. Rashwan et al. (2019) conducted a comprehensive review discussing the challenges and opportunities of sonohydrogen production ahead [21]. However, little has been done to explore the most effective acoustic and catalytic conditions [22–25]. To the best of our knowledge, only two works have reported sonochemical hydrogen production from seawater with an efficiency of 10.3 g_{cat}^{-1} L^{-1} Whr^{-1} (Qi et al. (2023)) and 3.0 μmol g_{cat}^{-1} L^{-1} Whr^{-1} (Harada et al. (2001)), respectively [26,27]. Furthermore, most of the reported sonochemical catalysts involve complex, costly, and energy intensive synthesis processes, which are difficult to scale in industrial processes. A few examples include Au/TiO_2, $La_{2x}Ga_{2y}In_{2(1-x-y)}O_3$, and Co_4N nanowires with N-defects [19,26,28].

In this article, we present an effective and sustainable strategy to convert water to hydrogen with cheap, corrosion resistant titanium dioxide (TiO_2) catalyst under high frequency ultrasound (780 kHz) at room temperature [29]. TiO_2 sonocatalyst exhibits high recyclability and corrosion resistance to seawater, maintaining a consistent hydrogen production rate. The system achieves a sonochemical efficiency of 8086 and 4210 μmol g_{cat}^{-1} L^{-1} Whr^{-1} with pure water and natural seawater, respectively, which both are the highest reported sonochemical hydrogen production rates in the literature. We further investigate the optimal acoustic and catalytic conditions for hydrogen production, including the number of cycles in pulsed ultrasound and catalyst concentration, and correlate the effects to a cavitation noise index. Moreover, the results are analysed using single bubble dynamics simulations and Electron Paramagnetic Resonance (EPR) to investigate the effects of a seawater environment on sonochemical hydrogen production, providing insights into both physical and chemical mechanisms influencing hydrogen generation. This paper promotes an effective approach in sonochemical hydrogen production, fostering its future development at a larger scale.

2. Materials and methods

This section details the materials, experimental setup, and methodologies used in this study. It includes the preparation of reaction solutions and reagents, measurement and processing of cavitation noise signals, and the analytical techniques employed to assess hydrogen production. Additionally, catalyst characterisation techniques and investigations into the effect of salt on sonochemical hydrogen production are presented, including single bubble simulations and EPR spectroscopy.

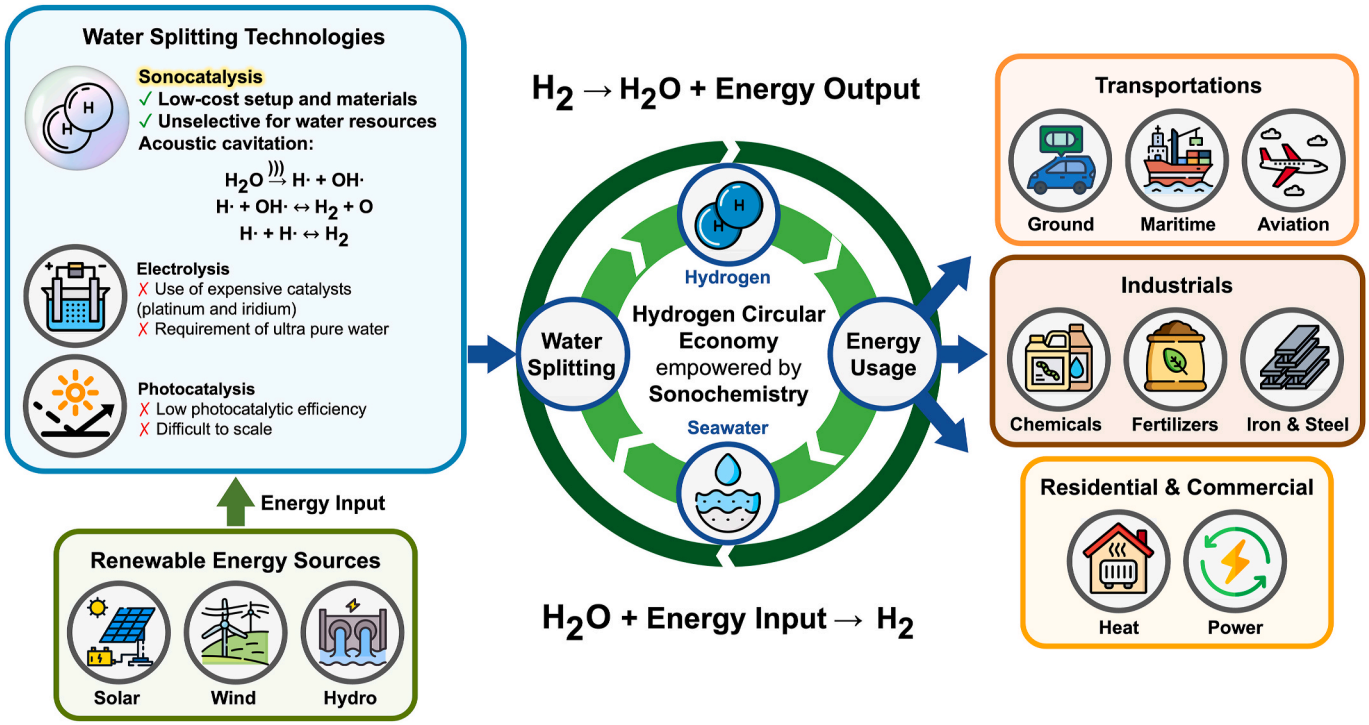

Fig. 1. Hydrogen circular economy enabled by sonochemistry. The hydrogen circular economy enabled by sonochemistry as an alternative hydrogen production technology. The technology is compared to water electrolysis and photocatalysis, which are well-discussed technologies for clean hydrogen production.

2.1. Materials

The following chemicals were used: Calcium chloride (anhydrous, granular, ≤7.0 mm, ≥93.0%, Sigma-Aldrich), Magnesium chloride (anhydrous for synthesis, Sigma-Aldrich), Potassium chloride (ACS reagent, 99.0–100.5%, Sigma-Aldrich), Sodium bicarbonate (ACS reagent, ≥99.7%, Sigma-Aldrich), Sodium chloride (ACS reagent, ≥99.0%, Sigma-Aldrich), Sodium sulfate (ACS reagent, ≥99.0%, Sigma-Aldrich), Titanium(IV) oxide (anatase, 99.6% metals basis, Thermo Scientific Chemicals). The gas used are as follows: Argon (Zero grade Ar, BOC), Helium (A Grade, 99.996%, BOC). De-ionised filtered Type 1 water (DI water) was obtained from a water purification system (Millipore Direct Q5-UV). The natural seawater was sourced from the Atlantic coast of Cornwall, United Kingdom, provided by Natural Seawater Supplier. The high purity spin trap agent 5,5-dimethyl-1-pyrroline-N-oxide (DMPO) (>99%) was purchased from Dojindo Molecular Technology Co., Ltd. All chemicals were used without further processing unless otherwise stated.

2.2. Sonochemical reactor system and measurement of cavitation noise signal

The experimental setup, schematically illustrated in Fig. 2, is composed of a 780 kHz sonochemical reactor with a maximum input power of 5.1 W (the maximum operating nominal power), alongside an acoustic cavitation noise measurement system [30]. In the system, radially spreading acoustic pulses were generated by a cylindrically tube transducer. The configuration of the reactor cylindrically focused the acoustic waves into a reactor vessel, creating a localised, intense acoustic pressure field for triggering sonochemical reactions. The transducers operating voltage and current were measured. Cavitation noise was recorded by a passive cavitation detector (PCD) and further analysed to determine the cavitation threshold and cavitation noise index. The hydrogen production was analysed via gas chromatography (GC). Catalysts used in this study were untreated commercially available TiO_2 particles. Using economical catalysts eliminated the need for expensive noble metals or adding energy-intensive complex catalyst synthesis processes.

The materials used for the construction of the reactor are described elsewhere [30]. The ultrasound transducer used was a cylindrical tube piezoelectric ceramic (Navy Type III (PKI802), lead zirconate titanate (PZT), Precision Acoustics Ltd) with a dimension of a dimension of 38 mm outer diameter, 34 mm inner diameter, 25 mm length, and a resonance frequency of 780 kHz. The transducer impedance and its power vs voltage relationship are shown in Supplementary Note 1.

The general experimental setup for sonochemical reaction and noise acquisition is described as follows: a waveform generator (Keysight Waveform Generator, 33600A) generated a pulsed of sine wave. The wave was fed through a −20 dB attenuator before being amplified by a 55 dB radiofrequency (RF) amplifier (Electronics & Innovation 1040L RF Amplifier), and finally transmitted to the ultrasound transducer to drive the sonochemical reaction. The driving voltage and current were measured and recorded with an oscilloscope with a sampling frequency of 100 MHz (TiePie Handyscope HS5 USB oscilloscope).

To detect cavitation noise, a PCD (Evident 384V-SU, 3.5 MHz, 0.25″, 1304373) was inserted into the cylindrical tube spacer through a hole. This spacer positioned the PCD directly beneath the polypropylene (PP) reaction vial. The noise signal received by PCD passed through a 1.8 MHz high-pass filter (Thor Labs High-Pass Filter 1.8 MHz, EF509), then into a 5 dB gain preamplifier (EG&G Instruments, Model 5185 Wideband Preamplifier) and a 50 Ω feed-through terminator (Tetratronix 011-0049-01 BNC Feed-Through Termination), and eventually to the oscilloscope. The oscilloscope was interfaced with a computer to record the noise data for subsequent data processing. A high-pass filter was employed to prevent the drive signal from overpowering the PCD signal, enabling the acquisition of frequencies larger than the drive signal. A terminator was used to match a 50 Ω impedance with the digital oscilloscope.

2.3. Reaction solution preparation and sonochemical reactions

2.5 mL reaction solution was used for every reaction using a 5 mL PP reaction vessel (round bottom test tube, Scientific Laboratory Supplies). The reaction solution for the sonochemical testing for acoustics and chemical optimisations were DI water with TiO_2 (0.3 mg/mL) unless otherwise specified. Simulated seawater was by prepared by dissolving NaCl, Na_2SO_4, KCl, and $NaHCO_3$ into DI water. The detailed composition of the simulated seawater is described in Supplementary Note 2.

Before every sonochemical reaction, the reaction solution and headspace were saturated with argon gas by purging the gas into the reaction solution for 5 min. All reactions were performed at ambient temperature and pressure. The standard operating frequency for the ultrasonic reaction was 780 kHz, reaction time was 20 min, duty cycle

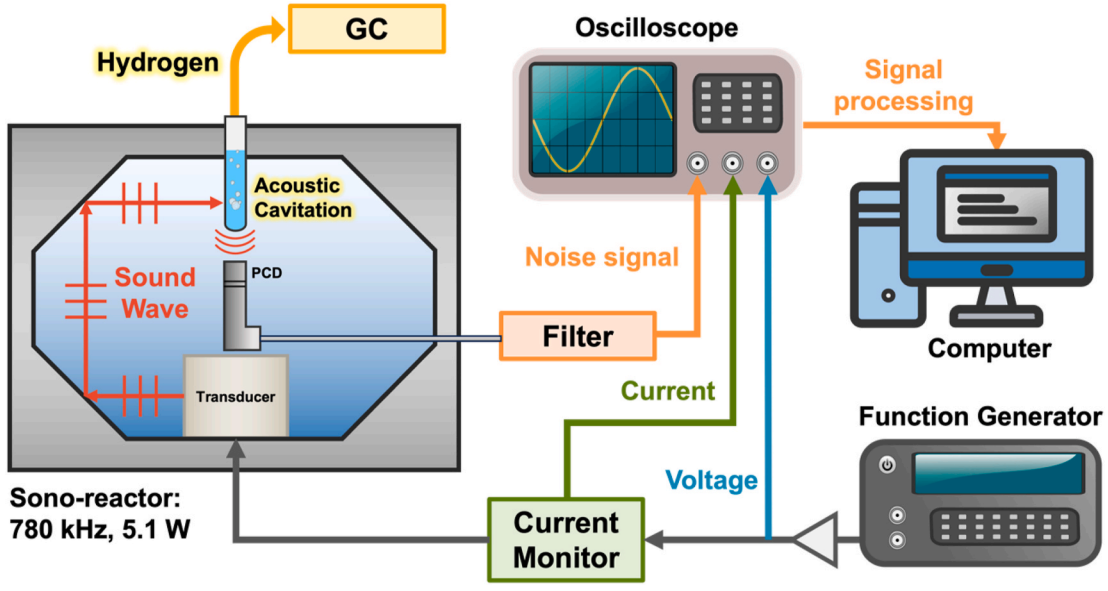

Fig. 2. Schematic of the reactor design and the experimental setup for the sonochemical hydrogen production, alongside an acoustic cavitation noise measurements system.

was 4.5% with 100 acoustic cycles and 2.849 ms burst period unless otherwise specified. The operating parameters for the sonochemical reactions are described in Supplementary Note 3.

2.4. Cavitation noise signal processing

The cavitation noise signal was snipped through the cavitating time window and transformed by Fast Fourier Transform (FFT) using the MATLAB function. The FFT spectrum was then integrated by the MATLAB trapezoidal numerical method to yield an integrated voltage value, V_{sample}. This operation was repeated by 100 bursts under a same trial; the 100 voltage values are averaged out then further averaged by at least two independent trials to obtain the sample average voltage value, $V_{avg\ sample}$. The same method was used to determine the average voltage value of the sonication of degassed water, $V_{avg\ degassed}$. Finally, the normalised cavitation noise index was obtained by equation (1).

$$\text{Normalised cavitation noise index (dB)} = 20 \bullet \log\left(\frac{V_{avg\ sample}}{V_{avg\ degassed}}\right) \quad (1)$$

2.5. Cavitation threshold determination

The cavitation threshold is defined as the minimal power at which cavitation is detected [31]. The cavitation noise index was measured and plotted against power (average operating power), and the data was fitted with a sigmoid fit followed equation (2).

$$\text{Cavitation noise index} = f(x) = (a\text{-}d)\left[e^{\left(-e^{(-b(x-c))}\right)}\right] \quad (2)$$

where f(x) is the normalised cavitation noise index, x is the power, and a, b, c, and d are the fitting parameters.

2.6. Hydrogen gas analysis

The amount of hydrogen was quantified using a GC (Shimadzu Nexis GC-2030) equipped with a dielectric-barrier discharge ionisation detector (BID) and helium (He) as carrier gas. A Carboxen®-1010 PLOT Capillary GC Column (Supelco, L × I.D. 30 m × 0.32 mm, average thickness 15 μm) was used as the analytical column. The GC-BID system was calibrated using an external standard method. The peak area of the GC signal was converted to the concentration of gas (ppm) using the calibration curve. The volume and number of moles of the hydrogen gas produced was estimated with the ideal gas law. The detailed analytical method is described in Supplementary Note 4 and an example calculation of hydrogen production is shown in Supplementary Note 5.

2.7. Collapse temperature estimation from single bubble simulation

Single spherical bubbles in water at different salinity were numerically investigated with the Keller-Miksis model that reads [32]:

$$(1-Ma)R\ddot{R} + \frac{3}{2}\left(1-\frac{\dot{Ma}}{3}\right)\dot{R}^2 = \frac{1}{\rho}(1+Ma)(p_l - p_\infty) + \frac{R}{\rho c}\frac{\partial p_l}{\partial t} \quad (3)$$

where R is the bubble radius, $Ma = \dot{R}c^{-1}$ is the Mach number, ρ is the liquid density, c is the speed of sound into the liquid, p_l is the liquid pressure at the bubble-liquid interface, and p_∞ is the liquid pressure in the far field. The dotting indicates a derivative in time. The interface pressure is as follows:

$$p_l = p_{b0}\left(\frac{R_0}{R}\right)^{3\gamma} - \frac{2S}{R} - \frac{4\mu\dot{R}}{R} \quad (4)$$

where γ is the heat capacity ratio set to 1.4, S is the surface tension, μ is the liquid viscosity. The model assumes adiabatic compression of the bubble contents of pressure p_{b0} at maximum expansion, made of non-condensable gas p_{g0} and water vapour p_v, the latter arbitrarily taken as 30% of the liquid vapour pressure at ambient temperature. The Keller-Miksis equation is solved with a fourth-order Runge-Kutta method. The collapse temperature is estimated with adiabatic assumption from a bubble of initial diameter of 25 μm, with p_{g0} of 10 Pa and an initial temperature of 25 °C [33]. The parameters used for the simulations are reported in Supplementary Note 6.

2.8. EPR spectroscopy

EPR spectra were measured at room temperature on a continuous-wave Bruker EMX micro spectrometer with an X-band frequency of 9.864 GHz. The detailed spectrometer parameters were as follows: central field of 3515 G; scanning width of 100 G; sweep time of 40 s with 16 number of scans; receiver gain of 64 dB; modulation amplitude of 1 G; microwave attention of 16 dB; microwave power of 5.024 mW. Samples solution with 25 mM DMPO were transferred to 50 μl quartz capillary tubes and then placed in the EPR cavity. EPR simulations were performed with easyspin package on MATLAB.

2.9. SEM images

The scanning electron microscope (SEM) images were obtained using a field emission gun scanning electron microscope (FEG-SEM, Zeiss Sigma 300) at an electron high tension voltage of 3.0 kV and a working distance of 4.6–4.7 mm.

3. Results and discussion

This section investigates the optimisation of sonochemical hydrogen production using TiO_2 catalysis, focusing on the effects of acoustic conditions and catalyst concentration. After identifying the optimal conditions, we extend our analysis to salty environments, including seawater, to examine how salt influences hydrogen production in the presence of TiO_2. The observed discrepancy between hydrogen production in pure and seawater is explored by evaluating both physical and chemical effects through single bubble simulations and radical analysis through EPR, respectively. Finally, our results are compared with previous studies in the literature to assess the relative performance and efficiency of our system.

3.1. Sonochemical hydrogen production

The reactor was operated under a constant duty cycle at 4.5%. This was to ensure that the ultrasound energy input remained unvaried at fixed reaction times across different exposure conditions. Additionally, the low duty cycle prevented the transducer from overheating and avoids thermal damage. At this constant duty cycle, we first investigated the impact of catalyst concentration, ultrasound pulse width, and ultrasound drive power.

Fig. 3 presents the results of hydrogen production optimised through chemical and acoustic parameters. Fig. 3a compares the hydrogen production rate in deionised (DI) water with and without the presence of TiO_2 catalyst, confirming the increases of hydrogen production rate by 25% compared when catalyst is used. Similarly to the production rate, a higher cavitation noise index has been recorded when TiO_2 is used. In line with previous studies, the phase boundaries between TiO_2 and water provides preferential sites for cavity bubble formation due to the decreased bubble nucleation energy barrier [34,35]. Therefore, heterogeneous nucleation mechanism increases cavitation activity in the presence of TiO_2 and is likely to be the primary mechanism that governs the improved sonocatalytic performance.

In addition to cavitation-induced reaction, TiO_2 photocatalytic and thermocatalytic processes may also enhance the rate by generating reaction species under light and heat, respectively [36,37]. As a semiconductor, TiO_2 generates electron-hole pairs (excitons), and consequently creates intermediate radicals such as •OH for hydrogen

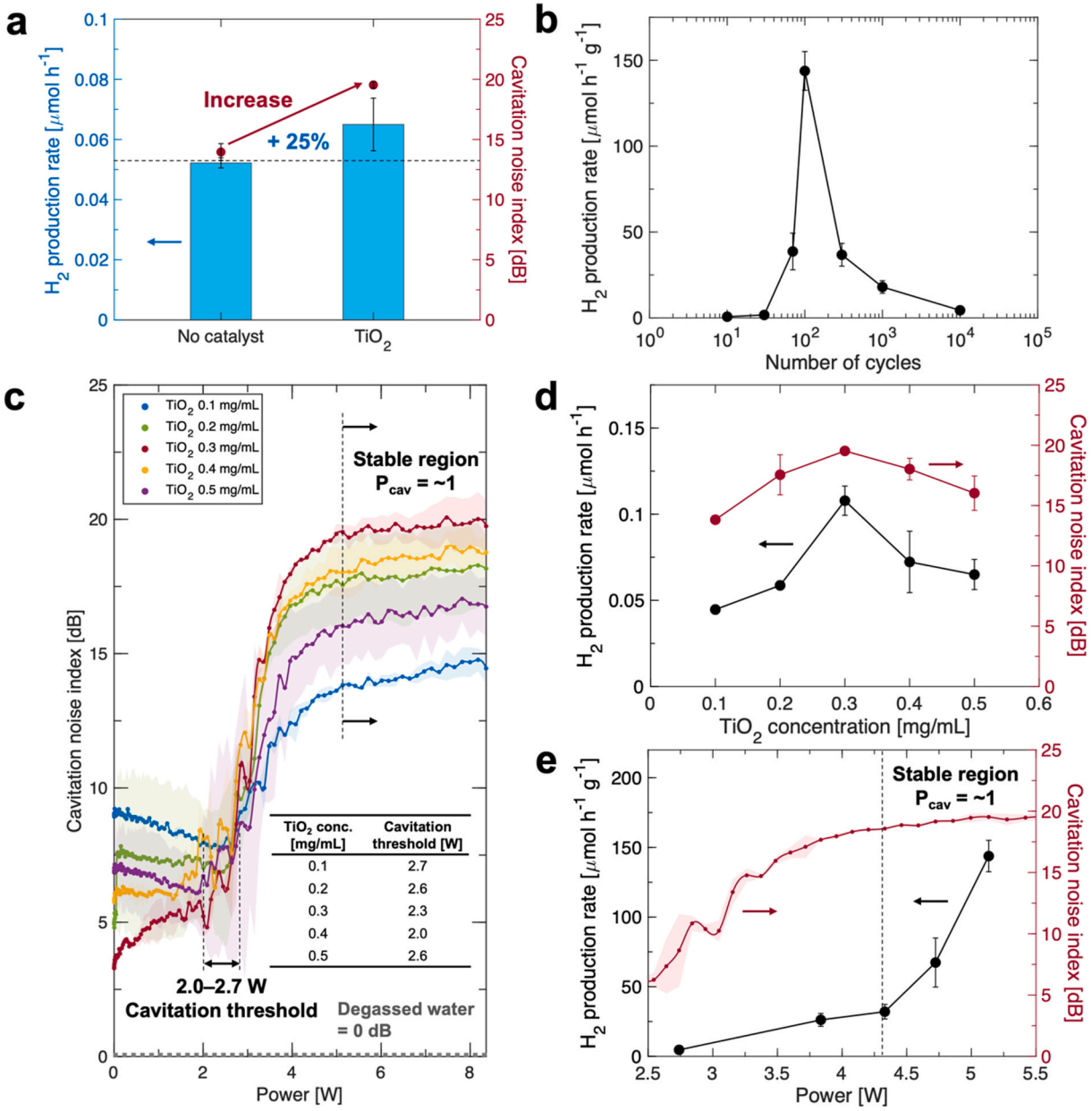

Fig. 3. Sonochemical hydrogen production with chemical and acoustic optimisations. **(a)** Hydrogen production rate (blue bar chart, left) and the cavitation noise index (red points, right) in absence and presence of TiO_2 (0.5 mg/mL). **(b)** Hydrogen production rate as a function of the number of acoustic cycles. **(c)** Average cavitation noise index as a function of power input across five TiO_2 concentrations, with the shaded region representing the standard deviation. **(d)** The hydrogen production rate (black points, left) and cavitation noise index (red points, right) as a function of TiO_2 concentration in solution. The lines are linear interpolation of the points for better illustration of the trend. **(e)** Hydrogen production rate (black points, left) and cavitation noise index (red points, right) as a function of power input. (For interpretation of the references to colour in this figure legend, the reader is referred to the Web version of this article.)

production when it absorbs sonoluminescent light (with energy higher than TiO_2 bandgap 3.2 eV) or under the extreme localised temperature in collapsing bubbles [38–40]. In this case, it remains unclear how much each process contributes to the total hydrogen production, especially since photocatalytic and thermocatalytic processes involve the formation of electron-hole pairs in the semiconductor, albeit triggered by different energy sources.

Fig. 3b shows hydrogen production rate as a function of the number of acoustic cycles. Data show that the optimal number of acoustic cycles is 100 which led to the largest hydrogen production rate. The experimental data is consistent with previous reported work with the same setup [30,41]. Below 100 cycles, there may not have been enough cycles to allow for the transducer to 'ring-up' and achieve maximum displacement and resulting in insufficient acoustic pressure to initiate inertial cavitation. Exceeding 100 cycles increases the time bubbles exist in the acoustic field, allowing for bubble-bubble interactions (e.g., coalescence) and rectified diffusion to occur. Ultimately, this may cause bubbles to grow excessively large, subsequently degassing the liquid medium [42].

We further investigated the acoustic cavitation response through different concentrations of sonocatalyst TiO_2 and reactor powers. The normalised cavitation noise index serves as a proxy for the acoustic cavitation activity at the reactant solution. Fig. 3c shows the cavitation noise index as a function of electrical drive power for different TiO_2 concentrations. Consistently with literature, the cavitation noise index has a sigmoidal shape over the range of electrical power [39,43]. For all TiO_2 concentrations investigated, the cavitation threshold was found in the range of 2.0–2.7 W. Details about the procedure for the

determination of the cavitation threshold from experimental data are in Supplementary Note 7. Interestingly, comparing the upper levelling off region of the curve, TiO_2 with a concentration of 0.3 mg/mL exhibits the highest cavitation noise index at around 20 dB. This suggests that 0.3 mg/mL may provide the optimal sonochemical performance compared to other concentrations. In fact, the hydrogen production rate as a function of TiO_2 concentration in solution, reported in Fig. 3d, shows that the optimal hydrogen production occurs at a TiO_2 concentration of 0.3 mg/mL. The observed trend is attributed to the effect of bubble populations. At a sub-optimal TiO_2 concentration (below 0.3 mg/mL), it is suggested that there are fewer bubble nucleation sites for the bubbles formation, causing a lower sonochemical rate. When the concentration of TiO_2 exceeds the optimal level, too many particles might absorb and scatter the sound waves. This scattering can shield the acoustic field reaching the focus area of the reactor. Furthermore, there may also be decoupling loss: the high concentration of sonocatalysts may alter the acoustic impedance of the medium and consequently cause the energy transfer efficiency from the transducer to the water to decrease [44].

Fig. 3e shows the sonochemical hydrogen production rate at different power inputs. The production rate increases particularly at the upper levelling off region (changes of cavitation noise index is nearly minimal beyond 4.3 W), indicating the cavitation probability (P_{cav}) is nearly unity [43]. The scaled cavitation probability curve vs input power is shown on Supplementary Figure 7.2. Although the cavitation probability at 4.3 W or higher is nearly unity, higher reactor power results in a greater acoustic pressure amplitude. This may cause a bigger bubble size just before implosion, which further causes higher cavitation temperature within hotspot, and an increase the bubble population, further enhancing radical production [45]. It is expected that the hydrogen production rate continues to increase beyond 5.1 W until the shielding and decoupling effect from the overcrowded bubble population come into play [44]. This was not tested because 5.1 W is the maximum safe operating power input for the transducer.

3.2. *Effect of seawater*

Next, we examined the effect of salts and different water sources on sonochemical hydrogen production using the optimised parameters identified earlier, focusing on how seawater composition and NaCl concentration influence the reaction. The results are presented in Fig. 4. Fig. 4a shows the sonochemical hydrogen production in presence of TiO_2 catalyst at the maximum concentration (0.3 mg/mL as discovered above) from DI water, natural seawater, artificial seawater, and artificial seawater. The superior hydrogen yield from DI water can be attributed to the lack of ions and salts, which may interfere with the sonochemical reactions by altering the chemical environment. Seawater have approximately half the yield of DI water. The presumed presence of organic microorganisms in these natural waters is deemed negligible on the cavitation generation process, evidenced by the similar hydrogen production rates between natural and artificial seawater. However, the generation of hydrogen peroxide through sonochemistry may sterilise the environment, reducing microorganism-related effects. Additionally, our exploration included hydrogen production from a 0.48 M NaCl solution, replicating the NaCl molarity of natural seawater. Simulated

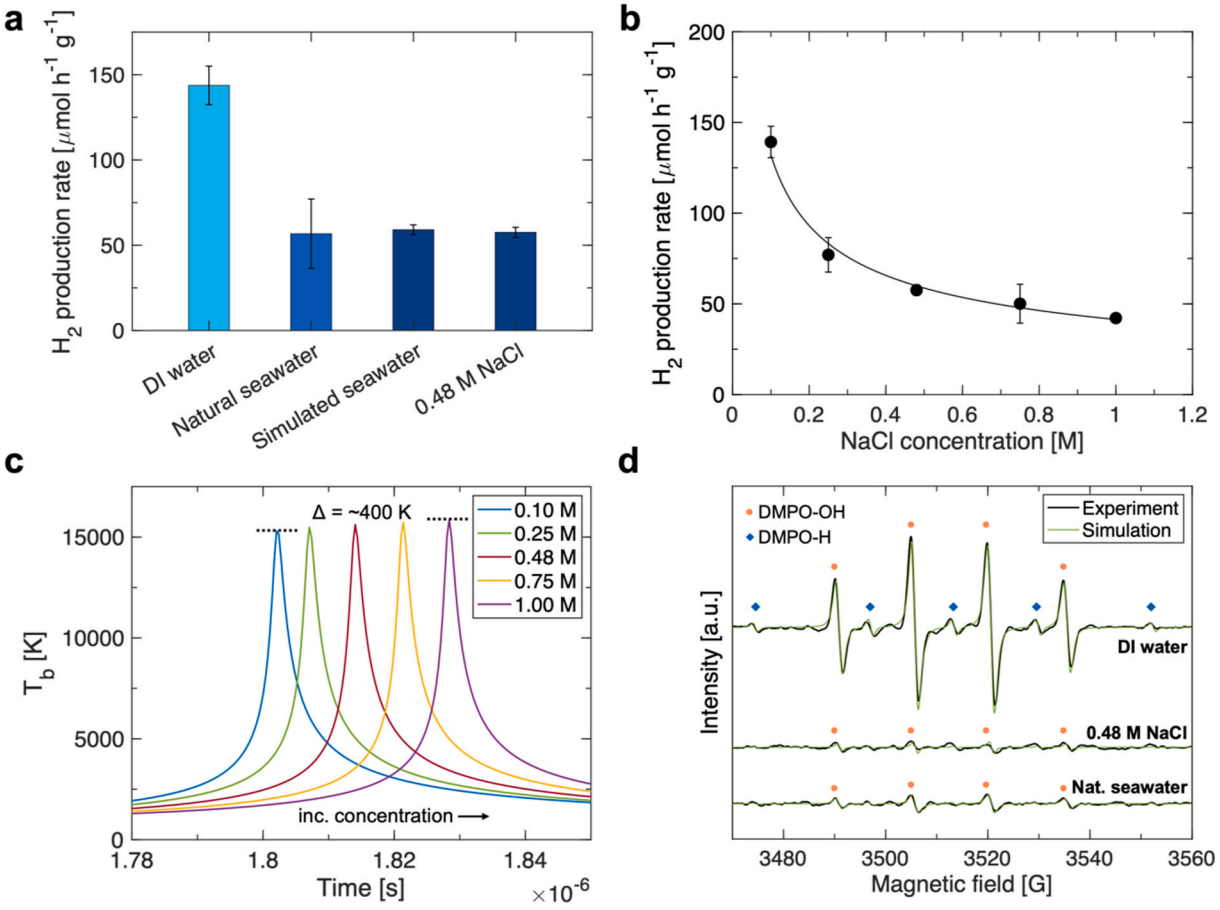

Fig. 4. Sonochemical hydrogen production under the effect of salts and different water resources. **(a)** Hydrogen production rate during sonication with water, natural seawater, simulated seawater, and 0.48 M NaCl solution. **(b)** The hydrogen production rate as a function of NaCl concentration in artificial seawater. **(c)** Simulations of bubble temperature at final collapse stage of a single cavitation bubble collapsing in solutions with different NaCl concentrations. **(d)** Experimental and simulated EPR spectra detected after sonication of DI water, artificial seawater, and natural seawater with the addition of 25 mM spin-trap DMPO.

seawater, composed of a 0.48 M NaCl solution along with other salts such as KCl, Na_2SO_4, and $NaHCO_3$, yields hydrogen at rates nearly identical to those from a solution containing only 0.48 M NaCl. This suggested that NaCl is the predominant salt influencing the sonochemical reactions due to its high concentration.

To elucidate why seawater yields less hydrogen production, we explored the effect of NaCl concentration on sonolysis. Fig. 4b, which shows the hydrogen production rate, reveals a decreasing trend with increasing NaCl concentrations. This decrease is attributed to a complex interplay of physical alterations and chemical reactions influenced by the NaCl concentration. Physically, NaCl modifies several properties of the solution, such as density, vapour pressure, viscosity, surface tension, and speed of sound [46,47]. These parameters were incorporated into a simulation of single spherical bubble dynamics to explore the bubble temperature during collapse at different NaCl concentrations.

Fig. 4c reports the temporal evolution of a bubble's internal temperature at the final stage of the collapse. Simulations are performed with the Keller-Miksis model for single spherical bubble under the assumption of adiabatic collapse. Results reveal that a higher NaCl concentrations increases the maximum temperature during bubble collapse. Although higher temperatures typically promote radical generations and hydrogen production, our experimental results paradoxically show a reduction in hydrogen yield [48,49], in contrast with simulations. It is to be noted that the temperature variation is relatively modest, with only a 400 K temperature difference between the 0.1 M and the 1 M solutions. However, the model does not account for mass transfer effects, which may be exacerbated by the presence of salt. Specifically, the evaporation at the bubble-liquid interface may increase the local salt concentration. Since the mass transfer of salt from the interface to the bulk liquid does not occur spontaneously, and vapour pressure inversely relates to salt concentration, this may slow down the rate of further vapour evaporating into the bubble, and hence causing less vapour reacts within the bubble at each cycle. Furthermore, increasing the salt concentration decreases the concentration of dissolved gas, i.e. argon, leading to less microbubble nuclei in the solutions, hence fewer sonochemically active bubbles [50]. Previous studies have demonstrated a positive correlation between the concentration of dissolved gases and the number of bubbles [48].

Chemical effects also contribute to the decreased hydrogen production in NaCl solution. The reactions may be represented as follows [51]:

$$NaCl \overset{)))}{\rightarrow} Na\bullet + Cl\bullet \quad (4)$$

$$Na\bullet + H_2O \rightarrow NaOH + H\bullet \quad (5)$$

$$Cl\bullet + H_2O \rightarrow HCl + OH\bullet \quad (6)$$

$$Na\bullet + OH\bullet \rightarrow NaOH \quad (7)$$

$$Na\bullet + H\bullet + M \rightarrow NaH + M \quad (8)$$

$$Cl\bullet + OH\bullet \rightarrow HOCl \quad (9)$$

$$Cl\bullet + H\bullet \rightarrow HCl \quad (10)$$

$$Cl\bullet + H_2 \rightarrow HCl + H\bullet \quad (11)$$

$$Na\bullet + Cl\bullet + M \rightarrow NaCl + M \quad (12)$$

At bubble collapse, salt molecules undergo a homolytic cleavage and release in its plasma form to produce Na• and Cl• (Equation (4)). These plasma species may subsequently react with water molecules and other water-based radicals, in turn impacting the overall yield of sonolysis. Possible reactions between these species are listed in Equations (5)–(12), where M denotes a third body in the reactions. A higher concentration of NaCl may increase the amount of Na• and Cl•, resulting in more H• and •OH radicals being scavenged and limiting the hydrogen production. This helps explaining the trend found in Fig. 4c.

EPR was also employed to investigate the NaCl scavenging effect in sonochemical hydrogen production. As H• and •OH radicals in solution have an extremely short half-life and are generally not directly detectable by EPR, indirect detection was performed at room temperature using spin-trapping with DMPO. To our delight, after sonication of DI water, natural seawater, and artificial seawater with the addition of 25 mM DMPO, we observe the formation of H• and •OH radicals (Fig. 4d). This aligns with findings in the literature, where the radicals are generated from water sonolysis during inertial cavitation [52]. The spectrum matches well with the EPR simulation, which is the sum of DMPO-OH (a_N = 14.9 G and a_H 14.9 G) and DMPO-H (a_N = 16.4 G and a_H 22.6 G), giving a_N and a_H values are in line with the DMPO-radical adduct. More details on the simulation are provided in Supplementary Note 8. It is also observed that that EPR spectra of natural and artificial seawater have a much smaller amplitude DMPO-OH spectrum lines and nearly no DMPO-H signal. This confirms that salt scavenges H• and •OH radicals, decreasing the hydrogen production compared to the case of DI water. It is to be noted that the EPR signal from natural seawater is slightly higher than the artificial solution. This is likely due to the trace amount of Fe ions presence in natural seawater, reacting with hydrogen peroxide as generated from water sonolysis and causing the generation of •OH radicals by Fenton chemistry. However, as the amount of Fe in seawater is nearly negligible (0.1–10 nM), the small amount of •OH radicals formed from Fenton chemistry may be ignored and conclude the presence of NaCl quenches H• and •OH radicals [53]. Considering this along with the physical effect, which demonstrates contrasting results by the above bubble simulation, chemical effect is likely to be the dominant effect for the decreased hydrogen yield under salty water.

3.3. Kinetics of sonocatalytic water splitting

We investigated the kinetics of sonocatalytic water splitting in DI water and natural seawater in presence of TiO_2. Fig. 5 illustrates the sonocatalytic hydrogen production rate and the recyclability of TiO_2 sonocatalyst. Fig. 5a shows the hydrogen concentration over time during sonication. The hydrogen production rate is 103.7 μmol g^{-1} h^{-1} in DI water and 54.0 μmol g^{-1} h^{-1} in natural seawater. The reaction is facilitated by the presence of TiO_2. In this heterogeneous catalytic reaction, the constant production rate likely indicates that the catalyst retained its activity and that the catalytic sites on the TiO_2 surface were fully utilised, at least in the sonication timespan investigated [54,55].

The pH variation during the sonication of DI water over time was also monitored (inset of Fig. 5a). The results show that during the reaction, the pH value gradually decreased from around 8 to 7. This trend suggests two simultaneous effects during the reaction. Initially, we observed the pH immediately following the sonochemical reaction consistently exceeded the initial pH = 7 of DI water, indicating a shift toward basicity [56]. This increase in basicity is attributed to the continuous consumption of hydrogen species from water molecules due to the formation of hydrogen gas. This process releases hydrogen gas into the gas phase, leaving behind OH species into the water, which increases the solution's basicity. pH is determined by the concentration of protons (H^+) and hydroxide ions (OH^-) in solution, while sonolysis produces H• and •OH radicals. The precise process by which electrons transfer from hydroxyl and hydrogen radicals to form hydrogen and hydroxide ions is still not fully understood. At the same time, despite the increasing concentration of OH species in the liquid phase, we observed a decrease in pH over time. This may be explained by the simultaneous production of a small amount of hydrogen peroxide during the cavitation process, which introduces acidic properties to the solution. Hydrogen peroxide, being a weak acid with a pH range of 3–6, counteracts the increase in basicity from the residual OH species, contributing to the gradual decrease in pH. The initial increase in basicity may also indicate that hydrogen peroxide forms more slowly than the consumption of hydrogen species during the sonochemical reactions.

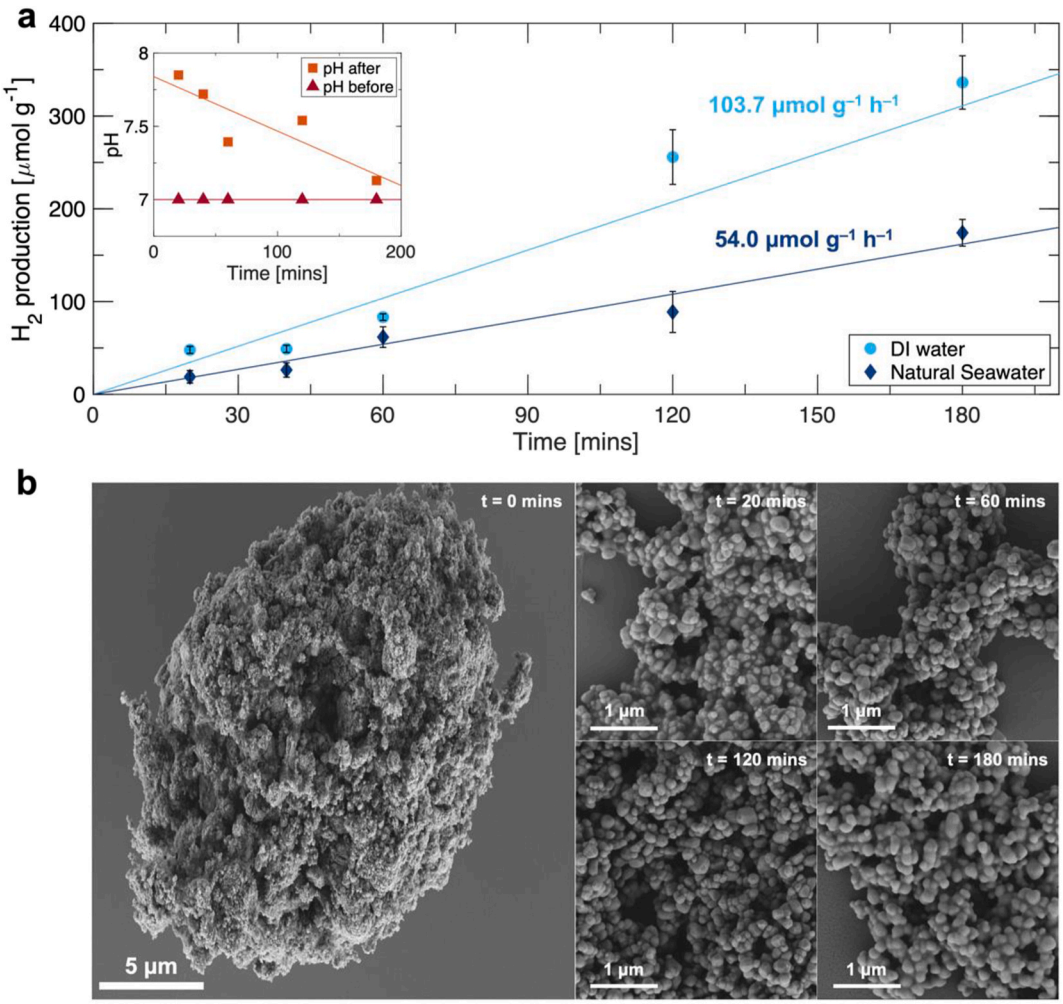

Fig. 5. Sonocatalytic hydrogen production rate and the recyclability of TiO_2 sonocatalyst. **(a)** Hydrogen generation yield in the function of reaction time for DI water and natural seawater. The error bars represent the standard deviation of three experimental trials for each reaction time. The hydrogen production rate was quantified by a linear fitting of hydrogen production over reaction time. The inlet figure shows the pH change over time for DI water with and without sonication. **(b)** SEM images of TiO_2 sonocatalysts at 0 min, 20 min, 60 min, 120 min, and 180 min for sonochemical seawater splitting.

Regarding the recyclability of the catalyst over the timespan of the reaction, TiO_2 catalyst experiences a significant reduction in particle size in the initial phase of sonication (0 min and 20 mins in Fig. 5b), thereby increasing the catalyst's surface area. It is expected that this initial size reduction enhances catalytic activity, as smaller particles provide more surface area and thus have greater availability of nucleation sites for cavitation bubbles, improving sonochemical efficiency [57,58]. This reduction in particle size is explained by the mechanical effects of inertial cavitation, including microjets and shock waves [59].

Following this initial ultrasonic fragmentation and surface modification, the particle's nanostructures remained a similar ball-like rough structure throughout the reaction time. This suggests that the catalyst preserves its nanoparticle structure under cavitating conditions for the reaction times studied here and supports the observed constant production rate described above. Moreover, this emphasises the potential recyclability and corrosion resistance of TiO_2 in different kinds of water.

3.4. Comparison with literature

We compared our system's sonocatalytic hydrogen production rate and sonochemical efficiency with those reported in existing literature across various operating frequencies, as detailed in Table 1 and illustrated in Fig. 6. The systems are categorised by the type of reaction solution used, including DI water and seawater. For a comprehensive comparison, we included other reactant solutions used in sonochemical hydrogen production, such as 10% and 20% ethanol/water mixtures. As depicted in Fig. 6, there are only 4 ultrasound frequencies available on the literature, no consistent trend in hydrogen production is observed with respect to frequency and solvent type with the little information available. This variability may indicate that factors like sonochemical reactor design, power input, catalyst type, and reactant volume significantly influence hydrogen production.

Fig. 6a indicates our system has a relatively low hydrogen production rate compared to the existing literature. It is crucial to note that each sonochemical system employs varying reactor volumes and power inputs. Therefore, to enable a fair comparison, the hydrogen production rate is normalised by the reaction volume and energy input. After normalising for these factors, our system displayed the highest sonochemical hydrogen production efficiency ever reported, as shown in Fig. 6b, an improvement of 10–100 times over existing literature. We attribute this superior performance of our system to the combination of an optimised TiO_2 catalyst concentration and acoustic parameter selection, and a reactor design that enhances cavitation activity through cylindrical converging ultrasound waves. Moreover, our results highlight the crucial role of scaling up reactant volumes for achieving large-scale sonochemical hydrogen production.

Table 1
Sonochemical hydrogen production results obtained from literature.

Reaction solution	Frequency [60]	Nominal power [W]	Gas	Reaction volume [L]	Catalysts	Concentration of catalysts [g/L]	Hydrogen production rate [μmol h^{-1} g^{-1}]	Normalised sonochemical efficiency [μmol g^{-1} L^{-1} Whr^{-1}]	Reference
DI water	40	50	Not stated	0.15	TiO_2	0.5	17.3	2.3	Wang, 2010
DI water	40	50	Not stated	0.15	Au/TiO_2	0.5	288.0	38.4	Wang, 2010
DI water	40	100	Argon	0.01	Co_4N nanowires with N-defect	0.5	28.5	28.5	Qi, 2023
DI water	200	200	Argon	0.3	TiO_2 rutile	0.7	250.0	4.2	Harada, 2001
DI water	200	200	Argon	0.1	Commercial TiO_2 powder	2.0	103.1	5.2	Harada, 2003
DI water	200	200	Argon	0.04	TiO_2 (Nippon Aerosil P-25)	5.0	210.6	26.3	Harada, 2001
DI water	200	200	Argon	0.04	MnO_2	5.0	72.9	9.1	Harada, 2001
DI water	**780**	**5.13**	**Argon**	**0.0025**	**TiO_2 anatase**	**0.3**	**103.7**	**8085.6**	**Current study, 2024**
Seawater	40	100	Argon	0.01	Co_4N nanowires with N-defect	0.5	10.3	10.3	Qi, 2023
Seawater (4% NaCl solution)	200	200	Argon	0.3	TiO_2 rutile	0.7	180.0	3.0	Harada, 2001
Seawater	**780**	**5.13**	**Argon**	**0.0025**	**TiO_2 anatase**	**0.3**	**54.0**	**4209.7**	**Current study, 2024**
10% ethanol/ water	38	50	Argon	0.2	$LaGa_{0.5}In_{0.5}O_3$	2.0	129.8	13.0	Gentili, 2009
10% ethanol/ water	38	50	Argon	1.1	$LaGa_{0.5}In_{0.5}O_3$	0.4	29.3	0.5	Gentili, 2009
10% ethanol/ water	38	50	Argon	0.2	$La_{0.8}Ga_{0.2}InO_3$	2.0	147.0	14.7	Gentili, 2009
10% ethanol/ water	38	50	Argon	1.1	$La_{0.8}Ga_{0.2}InO_3$	0.4	30.3	0.6	Gentili, 2009
10% ethanol/ water	38	50	Argon	0.2	$S:La_{0.8}Ga_{0.2}InO_3$	2.0	177.0	17.7	Gentili, 2009
10% ethanol/ water	38	50	Argon	1.1	$S:La_{0.8}Ga_{0.2}InO_3$	0.4	38.3	0.7	Gentili, 2009
20% ethanol/ water	38	2.6	Argon	0.3	$S:Y_{0.8}Ga_{0.2}InO_3$	1.3	267.5	342.9	Penconi, 2015

4. Conclusions

Current study demonstrated that ultrasound-driven water and seawater splitting catalysed by TiO_2 is an effective approach for hydrogen production. We identified that the optimal TiO_2 concentration of 0.3 mg/mL, as determined experimentally and validated by cavitation noise signal measurements using a PCD and signal processing methods, plays a crucial role in enhancing sonochemical hydrogen production. Additionally, 100 was determined to be the optimal number of acoustic cycles in pulsed ultrasound, which further improves hydrogen yield. After establishing optimal operating conditions, we elucidated that the presence of salt significantly decreases hydrogen production due to both physical and chemical effects. Based on our results from bubble dynamics simulations and EPR measurements, the chemical salt-scavenging effect appears to be the dominant factor in reducing efficiency rather than physical effects. Our system (780 kHz, 5.1 W) achieved the highest reported normalised sonochemical hydrogen production efficiency across the literature for pure and natural seawater, with values of 8086 and 4210 μmol g_{cat}^{-1} L^{-1} Whr^{-1}, respectively. Alternatively, these hydrogen production rates can also be expressed as 103.7 μmol h^{-1} g^{-1} for pure water and 52 μmol h^{-1} g^{-1} for seawater. We believe this current study can guide further development in sonochemical hydrogen production and potentially enable the technology to compete with and complement traditional hydrogen production methods.

CRediT authorship contribution statement

Cherie C.Y. Wong: Writing – original draft, Visualization, Project administration, Methodology, Investigation, Formal analysis, Data curation, Conceptualization. **Davide Bernardo Preso:** Writing – review & editing, Writing – original draft, Software, Formal analysis. **Yi Qin:** Writing – review & editing, Investigation. **Pankaj S. Sinhmar:** Writing – review & editing, Methodology. **Zhiyuan Zong:** Methodology. **James Kwan:** Writing – review & editing, Supervision, Funding acquisition, Conceptualization.

Declaration of competing interest

The authors declare that they have no known competing financial

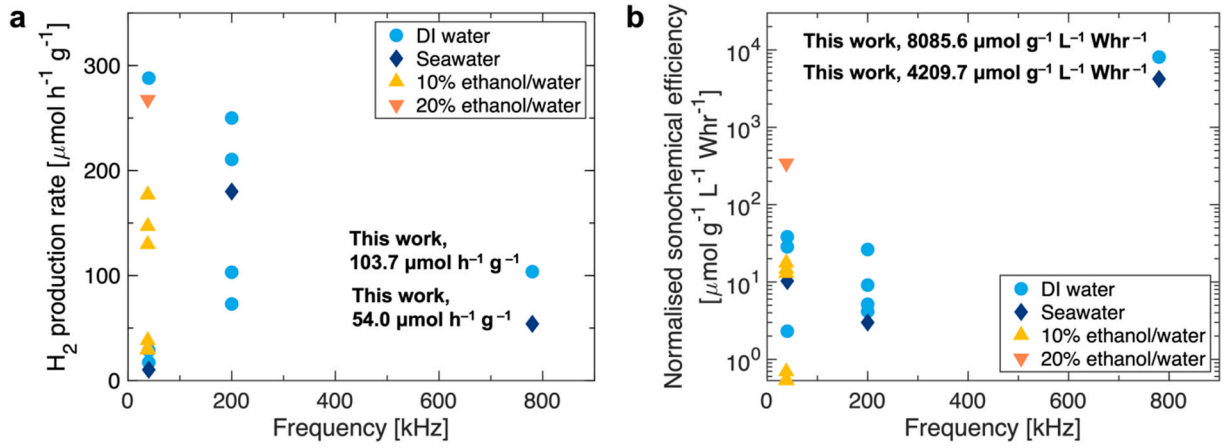

Fig. 6. Sonochemical hydrogen production rate and the type of reaction solutions in comparison to the existing literature. **(a)** Sonochemical hydrogen production rate (μmol h^{-1} g^{-1}) vs the operating frequency of the sonochemical reactor. The production rate is categorised by the type of reaction solutions. (**b)** Sonochemical efficiency after being normalised by the mass of catalyst used and input energy (μmol g^{-1} L^{-1} Whr^{-1}) vs the operating frequency. Our system represents the highest reported sonochemical hydrogen production rate with 10–100 times improvement compared to the current literature.

interests or personal relationships that could have appeared to influence the work reported in this paper.

Acknowledgements

C. C. Y. W. thanks the Department of Engineering Science (University of Oxford) and Balliol College, University of Oxford) for their support through the EPSRC Doctoral Training Partnerships (DTP) Scholarship and the Dervouguilla Scholarship, respectively. Current study was supported by the Engineering and Physical Sciences Research Council (Grant Reference EP/W012316/1) and EPSRC UKRI Impact Acceleration Account Award (Grant Reference EP/X525777/1).

Nomenclature

Symbol/Abbreviation	Full Term
a	Hyperfine coupling constants (G)
a_H	Hyperfine coupling constant for hydrogen nuclei (G)
a_N	Hyperfine coupling constant for nitrogen nuclei (G)
BID	Dielectric-barrier discharge ionisation detector
c	Speed of sound into the liquid (m/s)
DI water	Deionised water
DMPO	5,5-Dimethyl-1-pyrroline-N-oxide
EPR	Electron paramagnetic resonance
FEG-SEM	Field emission gun scanning electron microscope
FFT	Fast Fourier Transform
GC	Gas chromatography
H^+	Protons
H_2	Molecular hydrogen
H_2O_2	Hydrogen peroxide
He	Helium
Ma	Mach number (*Ma*)
NaCl	Sodium chloride
OH^-	Hydroxide ions
P_{cav}	Cavitation probability
p_{b0}	Liquid pressure at the bubble contents at maximum expansion (Pa)
p_{g0}	Liquid pressure of the non-condensable gas (Pa)
p_I	Liquid pressure at the bubble-liquid interface (Pa)
p_v	Liquid pressure of water vapour (Pa)
p_∞	Liquid pressure in the far field (Pa)
PCD	Passive cavitation detector
PP	Polypropylene
ppm	Part per million (ppm)
PZT	Lead zirconate titanate
R	Radius (m)
RF	Radiofrequency
S	Surface tension (N/m)
SEM	Scanning electron microscopy
T	Temperature (K or °C)
t	Time (mins)
TiO_2	Titanium dioxide
V	Voltage (V)
$V_{avg\ sample}$	Sample average voltage value (V)
$V_{avg\ degassed}$	Degassed water average voltage value (V)

(*continued on next page*)

(*continued*)

Symbol/Abbreviation	Full Term
Δ	Change in quantity
γ	Heat capacity ratio
μ	Liquid viscosity (Pa·s)
ρ	Liquid density (g/mL)

Appendix A. Supplementary data

Supplementary data to this article can be found online at https://doi.org/10.1016/j.ijhydene.2025.02.327.

References

[1] Khaligh V, Ghezelbash A, Akhtar MS, Zarei M, Liu J, Won W. Optimal integration of a low-carbon energy system – a circular hydrogen economy perspective. Energy Convers Manag 2023;292:117354. https://doi.org/10.1016/j.enconman.2023.117354.

[2] Kabir MM, Akter MM, Huang Z, Tijing L, Shon HK. Hydrogen production from water industries for a circular economy. Desalination 2023;554:116448. https://doi.org/10.1016/j.desal.2023.116448.

[3] Jin H, Xu J, Liu H, Shen H, Yu H, Jaroniec M, Zheng Y, Qiao S-Z. Emerging materials and technologies for electrocatalytic seawater splitting. Sci Adv 2023;9:eadi7755. https://doi.org/10.1126/sciadv.adi7755.

[4] Xu S-W, Li J, Zhang N, Shen W, Zheng Y, Xi P. Recent advances in direct seawater splitting for producing hydrogen. Chem Commun 2023;59:9792–802. https://doi.org/10.1039/D3CC02074F.

[5] Li C, Baek J-B. Recent advances in noble metal (Pt, Ru, and Ir)-Based electrocatalysts for efficient hydrogen evolution reaction. ACS Omega 2020;5:31–40. https://doi.org/10.1021/acsomega.9b03550.

[6] Salonen LM, Petrovykh DY, Kolen'ko YV. Sustainable catalysts for water electrolysis: selected strategies for reduction and replacement of platinum-group metals. Mater Today Sustain 2021;11–12:100060. https://doi.org/10.1016/j.mtsust.2021.100060.

[7] Dresp S, Dionigi F, Klingenhof M, Merzdorf T, Schmies H, Drnec J, Poulain A, Strasser P. Molecular understanding of the impact of saline contaminants and alkaline pH on NiFe layered double hydroxide oxygen evolution catalysts. ACS Catal 2021;11:6800–9. https://doi.org/10.1021/acscatal.1c00773.

[8] Guo J, Zheng Y, Hu Z, Zheng C, Mao J, Du K, Jaroniec M, Qiao S-Z, Ling T. Direct seawater electrolysis by adjusting the local reaction environment of a catalyst. Nat Energy 2023;8:264–72. https://doi.org/10.1038/s41560-023-01195-x.

[9] Gao F-Y, Yu P-C, Gao M-R. Seawater electrolysis technologies for green hydrogen production: challenges and opportunities. Curr Opin Chem Eng 2022;36:100827. https://doi.org/10.1016/j.coche.2022.100827.

[10] Dresp S, Dionigi F, Klingenhof M, Strasser P. Direct electrolytic splitting of seawater: opportunities and challenges. ACS Energy Lett 2019;4:933–42. https://doi.org/10.1021/acsenergylett.9b00220.

[11] Dang V-H, Nguyen T-A, Le M-V, Nguyen DQ, Wang YH, Wu JCS. Photocatalytic hydrogen production from seawater splitting: current status, challenges, strategies and prospective applications. Chem Eng J 2024;484:149213. https://doi.org/10.1016/j.cej.2024.149213.

[12] Leong TSH, Manickam S, Martin GJ, Li W, Ashokkumar M. Ultrasonic production of nano-emulsions for bioactive delivery in drug and food applications. Springer; 2018.

[13] Suslick KS. Sonochemistry. Science 1990;247:1439–45. https://doi.org/10.1126/science.247.4949.1439.

[14] Ziembowicz S, Kida M, Koszelnik P. Sonochemical Formation of hydrogen peroxide. Proceedings 2018;2:188. https://doi.org/10.3390/ecws-2-04957.

[15] Ziembowicz S, Kida M, Koszelnik P. The impact of selected parameters on the formation of hydrogen peroxide by sonochemical process. Separ Purif Technol 2018;204:149–53. https://doi.org/10.1016/j.seppur.2018.04.073.

[16] Meroni D, Djellabi R, Ashokkumar M, Bianchi CL, Boffito D C Sonoprocessing. From concepts to large-scale reactors. Chem Rev 2021. https://doi.org/10.1021/acs.chemrev.1c00438.

[17] Zhang T, Guan X, Zhu B, Zhang Z, Ye X, Zeng W, Gao Z, Guo L. Boosting solar-driven thermal-assisted photocatalytic hydrogen production through device thermal management. Int J Hydrogen Energy 2024;51:921–34. https://doi.org/10.1016/j.ijhydene.2023.07.103.

[18] Zhang X, Xu C, Zhang L, Li Z, Hong J, Zhang Y. Photothermal catalytic water splitting at diverse two-phase interfaces based on Cu–TiO2. ACS Appl Energy Mater 2022;5:4564–76. https://doi.org/10.1021/acsaem.2c00009.

[19] Gentili PL, Penconi M, Ortica F, Cotana F, Rossi F, Elisei F. Synergistic effects in hydrogen production through water sonophotolysis catalyzed by new La2xGa2yIn2(1−x−y)O3 solid solutions. Int J Hydrogen Energy 2009;34:9042–9. https://doi.org/10.1016/j.ijhydene.2009.09.027.

[20] Penconi M, Rossi F, Ortica F, Elisei F, Gentili PL. Hydrogen production from water by photolysis, sonolysis and sonophotolysis with solid solutions of rare earth, gallium and indium oxides as heterogeneous catalysts. Sustainability 2015;7:9310–25. https://doi.org/10.3390/su7079310.

[21] Rashwan SS, Dincer I, Mohany A, Pollet BG. The Sono-Hydro-Gen process (Ultrasound induced hydrogen production): challenges and opportunities. Int J Hydrogen Energy 2019;44:14500–26. https://doi.org/10.1016/j.ijhydene.2019.04.115.

[22] Merouani S, Hamdaoui O. The sonochemical approach for hydrogen production. Springer International Publishing; 2020.

[23] Islam MH, Burheim OS, Pollet BG. Sonochemical and sonoelectrochemical production of hydrogen. Ultrason Sonochem 2019;51:533–55. https://doi.org/10.1016/j.ultsonch.2018.08.024.

[24] Sharifishourabi M, Dincer I, Mohany A. Experimental testing of a novel sonic method for clean hydrogen generation. Int J Hydrogen Energy 2024;82:206–17. https://doi.org/10.1016/j.ijhydene.2024.07.378.

[25] Sharifishourabi M, Dincer I, Mohany A. Implementation of experimental techniques in ultrasound-driven hydrogen production: a comprehensive review. Int J Hydrogen Energy 2024;62:1183–204. https://doi.org/10.1016/j.ijhydene.2024.03.013.

[26] Qi W, Liu J, Guo X, Guo H, Thomas T, Zhu Y, Liu S, Yang M. Vacancy-defective cobalt nitride nanostructures for sonocatalytic hydrogen production using various water resources. ACS Appl Nano Mater 2023;6:2636–45. https://doi.org/10.1021/acsanm.2c05054.

[27] Harada H. Isolation of hydrogen from water and/or artificial seawater by sonophotocatalysis using alternating irradiation method. Int J Hydrogen Energy 2001;26:303–7. https://doi.org/10.1016/S0360-3199(00)00095-1.

[28] Wang Y, Zhao D, Ji H, Liu G, Chen C, Ma W, Zhu H, Zhao J. Sonochemical hydrogen production efficiently catalyzed by Au/TiO2. J Phys Chem C 2010;114:17728–33. https://doi.org/10.1021/jp105691v.

[29] Mardare L, Benea L. Effects of TiO2 nanoparticles on the corrosion protection ability of polymeric primer coating system. Polymers 2021;13:614. https://doi.org/10.3390/polym13040614.

[30] Wong CCY, Raymond JL, Usadi LN, Zong Z, Walton SC, Sedgwick AC, Kwan J. Enhancement of sonochemical production of hydroxyl radicals from pulsed cylindrically converging ultrasound waves. Ultrason Sonochem 2023;99:106559. https://doi.org/10.1016/j.ultsonch.2023.106559.

[31] Kyriakou Z, Corral-Baques MI, Amat A, Coussios C-C. HIFU-induced cavitation and heating in ex vivo porcine subcutaneous fat. Ultrasound Med Biol 2011;37:568–79. https://doi.org/10.1016/j.ultrasmedbio.2011.01.001.

[32] Keller JB, Miksis M. Bubble oscillations of large amplitude. J Acoust Soc Am 1980;68:628–33. https://doi.org/10.1121/1.384720.

[33] Preso DB, Fuster D, Sieber AB, Obreschkow D, Farhat M. Vapor compression and energy dissipation in a collapsing laser-induced bubble. Phys Fluids 2024;36. https://doi.org/10.1063/5.0200361.

[34] Shchukin DG, Skorb E, Belova V, Möhwald H. Ultrasonic cavitation at solid surfaces. Adv Mater 2011;23:1922–34. https://doi.org/10.1002/adma.201004494.

[35] Doktycz SJ, Suslick KS. Interparticle collisions driven by ultrasound. Science 1990;247:1067–9. https://doi.org/10.1126/science.2309118.

[36] Qiu P, Park B, Choi J, Thokchom B, Pandit AB, Khim J. A review on heterogeneous sonocatalyst for treatment of organic pollutants in aqueous phase based on catalytic mechanism. Ultrason Sonochem 2018;45:29–49. https://doi.org/10.1016/j.ultsonch.2018.03.003.

[37] Wang G, Cheng H. Application of photocatalysis and sonocatalysis for treatment of organic dye wastewater and the synergistic effect of ultrasound and light. Molecules 2023;28:3706. https://doi.org/10.3390/molecules28093706.

[38] Ogi H, Hirao M, Shimoyama M. Activation of TiO2 photocatalyst by single-bubble sonoluminescence for water treatment. Ultrasonics 2002;40:649–50. https://doi.org/10.1016/S0041-624X(02)00191-9.

[39] Jonnalagadda US, Su X, Kwan JJ. Nanostructured TiO2 cavitation agents for dual-modal sonophotocatalysis with pulsed ultrasound. Ultrason Sonochem 2021:105530. https://doi.org/10.1016/j.ultsonch.2021.105530.

[40] Matsumoto K, Sato Y, Ebara T, Mizuguchi J. Hydrogen production from methanol or methane by the use of thermally generated holes in TiO2. J Chem Eng Jpn 2008;41:57–61. https://doi.org/10.1252/jcej.07we234.

[41] Zong Z, Gilbert E, Wong CCY, Usadi L, Qin Y, Huang Y, Raymond J, Hankins N, Kwan J. Efficient sonochemical catalytic degradation of tetracycline using TiO2 fractured nanoshells. Ultrason Sonochem 2023;101:106669. https://doi.org/10.1016/j.ultsonch.2023.106669.

[42] Tuziuti T, Yasui K, Lee J, Kozuka T, Towata A, Iida Y. Mechanism of enhancement of sonochemical-reaction efficiency by pulsed ultrasound. J Phys Chem 2008;112:4875–8. https://doi.org/10.1021/jp802640x.
[43] Maxwell AD, Cain CA, Hall TL, Fowlkes JB, Xu Z. Probability of cavitation for single ultrasound pulses applied to tissues and tissue-mimicking materials. Ultrasound Med Biol 2013;39:449–65. https://doi.org/10.1016/j.ultrasmedbio.2012.09.004.
[44] Iersel MMv, Benes NE, Keurentjes JTF. Importance of acoustic shielding in sonochemistry. Ultrason Sonochem 2008;15:294–300. https://doi.org/10.1016/j.ultsonch.2007.09.015.
[45] Toegel R, Gompf B, Pecha R, Lohse D. Does water vapor prevent upscaling sonoluminescence? Phys Rev Lett 2000;85:3165–8. https://link.aps.org/doi/10.1103/PhysRevLett.85.3165.
[46] Schumpe A. The estimation of gas solubilities in salt solutions. Chem Eng Sci 1993;48:153–8. https://doi.org/10.1016/0009-2509(93)80291-W.
[47] Gonçalves FA, Kestin J. The viscosity of NaCl and KCl solutions in the range 25–50°C. Ber Bunsen Ges Phys Chem 1977;81:1156–61. https://doi.org/10.1002/bbpc.19770811108.
[48] Brotchie A, Statham T, Zhou M, Dharmarathne L, Grieser F, Ashokkumar M. Acoustic bubble sizes, coalescence, and sonochemical activity in aqueous electrolyte solutions saturated with different gases. Langmuir 2010;26:12690–5. https://doi.org/10.1021/la1017104.
[49] Pflieger R, Nikitenko SI, Ashokkumar M. Effect of NaCl salt on sonochemistry and sonoluminescence in aqueous solutions. Ultrason Sonochem 2019;59:104753. https://doi.org/10.1016/j.ultsonch.2019.104753.
[50] Agarwal K, Trivedi M, Nirmalkar N. Does salting-out effect nucleate nanobubbles in water: spontaneous nucleation? Ultrason Sonochem 2022;82:105860. https://doi.org/10.1016/j.ultsonch.2021.105860.
[51] Lepoint-Mullie F, Voglet N, Lepoint T, Avni R. Evidence for the emission of 'alkali-metal–noble-gas' van der Waals molecules from cavitation bubbles. Ultrason Sonochem 2001;8:151–8. https://doi.org/10.1016/S1350-4177(00)00030-4.
[52] Kohno M, Mokudai T, Ozawa T, Niwano Y. Free radical formation from sonolysis of water in the presence of different gases. J Clin Biochem Nutr 2011;49:96–101. https://doi.org/10.3164/jcbn.10-130.
[53] John SG, Adkins JF. Analysis of dissolved iron isotopes in seawater. Mar Chem 2010;119:65–76. https://doi.org/10.1016/j.marchem.2010.01.001.
[54] Kumari N, Mahata A, Chakraborty B. Immobilization of phosphamide on the TiO2 surface for heterogeneous phase catalytic appel reaction. Inorg Chem 2023;62:7728–37. https://doi.org/10.1021/acs.inorgchem.3c00304.
[55] Fernández-Pérez A, Marbán G. Titanium dioxide: a heterogeneous catalyst for dark peroxidation superior to iron oxide. J Environ Chem Eng 2020;8:104254. https://doi.org/10.1016/j.jece.2020.104254.
[56] Vikulin, P. & Vikulina, V. in *IOP conference series: materials Science and engineering*. 042007 (IOP Publishing).
[57] Sasikala R, Jayakumar OD, Kulshreshtha SK. Enhanced hydrogen generation by particles during sonochemical decomposition of water. Ultrason Sonochem 2007;14:153–6. https://doi.org/10.1016/j.ultsonch.2006.06.005.
[58] Soleimani F, Madaah Hosseini HR, Ordikhani F, Mokhtari-Dizaji M. Enhancing sonocatalytic properties of TiO2 nanocatalysts by controlling the surface conditions: effect of particle size and PVA modification. Desalination Water Treat 2016;57:28378–85. https://doi.org/10.1080/19443994.2016.1185746.
[59] Li Z, Zhuang T, Dong J, Wang L, Xia J, Wang H, Cui X, Wang Z. Sonochemical fabrication of inorganic nanoparticles for applications in catalysis. Ultrason Sonochem 2021;71:105384. https://doi.org/10.1016/j.ultsonch.2020.105384.
[60] Asakura Y, Nishida T, Matsuoka T, Koda S. Effects of ultrasonic frequency and liquid height on sonochemical efficiency of large-scale sonochemical reactors. Ultrason Sonochem 2008;15:244–50. https://doi.org/10.1016/j.ultsonch.2007.03.012.